Detection of mutual phase synchronization in multivariate signals and application to phase ensembles and chaotic data

A. Hutt*
Weierstrass-Institute for Applied Analysis and Stochastics, Mohrenstrasse 39, 10117 Berlin, Germany

A. Daffertshofer†
Faculty of Human Movement Sciences, Vrije Universiteit, Van der Boechorststraat 9, 1081 BT Amsterdam, The Netherlands

U. Steinmetz‡
Max-Planck-Institute for Mathematics in the Sciences, Inselstrasse 22-26, 04103 Leipzig, Germany

(Received 24 April 2003; published 30 September 2003)

This work presents a method for the detection of mutual phase synchronization in nonstationary time series. We show how the application of a cluster algorithm that considers spatiotemporal structures of data follows from the general condition of phase-synchronized data. In view of the topology of phasic data, we reformulate the *K*-means cluster algorithm on a flat torus and apply a segmentation index derived in an earlier work [A. Hutt and H. Riedel, Physica D **177**, 203 (2003)]. This index is extended by means of averaging in order to reflect phase synchronization in ensembles of multivariate time series. The method is illustrated using simulated multivariate phase dynamics and arrays of chaotic systems, in which temporal segments of phase-synchronized states are registered. A comparison with results from an existing bivariate synchronization index reveals major advantages of our method.

DOI: 10.1103/PhysRevE.68.036219 PACS number(s): 05.45.Xt, 02.50.Sk, 05.10.−a

I. INTRODUCTION

To gain insight into the underlying dynamical mechanisms, the temporal activity in spatially extended systems needs to be measured. Experimental studies aiming for the extraction of spatiotemporal activity usually apply sets of spatially distributed detectors that yield multivariate time series, as can be appreciated in several studies in neuroscience [1–3], chemistry [4], meteorology [5], and solid state physics [6,7]. Extracting and understanding of the underpinning dynamics in a generality is far from trivial. For instance, in the case of thermodynamically open systems, empirical data typically contain various time scales, which complicates the modeling of data, as many models basically cover rather narrow bands of time scales. However, data recorded in certain open systems might be split into temporal sequences of fast transients on the one hand and time windows of narrow-band time scales on the other. Such phenomena are prominent, for example, in cognitive neuroscience [8], hydrodynamics [9,10], lasers physics [11,12], or in various chaotic systems [13,14].

A general framework addressing this issue is given by concepts of coherence or synchronization. In recent years, large achievements led to conceptually new approaches to biological systems [15–18] or, more generically, in networks of coupled oscillatory systems [19–23]. A system's behavior that alternates in time as mentioned before, i.e., fast transients versus narrow-band time scales, can be generalized to alternations between transients and synchronized states. To detect the resulting segments in time, several works investigated global amplitude coherence in nonstationary multivariate time series [8,24–29]. Indeed, these phenomena typically exhibit both a single mutual increase and a mutual decrease of amplitudes, that is, they do not oscillate in time. With respect to synchronization, however, this behavior is equivalent to mutual phase synchronization if all amplitudes are in phase. Since phase synchronization plays an important role in complex systems [4,17,18,30], we put all the previously listed phenomena in this, more general context and treat the detection of quasistationary mutual phase synchronization (see, e.g., Refs. [17,31–33]).

Starting with time series of amplitudes, corresponding time-dependent phase angles may be obtained from a wavelet analysis, via the Gabor transformation, or via the Hilbert transformation. Widely used indices for $n:m$ phase synchronization are the circular variance of phases and tests on statistical distributions of phases [31,34–37]. In fact, all these methods apply to bivariate data, whereas in the present study we treat multivariate data. For this kind of setups one can find several studies considering averaged phases [34,35] but, unfortunately, they commonly neglect eventually heterogeneous phase distributions. To the best of our knowledge, a reliable detection method for mutual phase synchronization in multivariate data has not been derived yet. Notice that, in general, phase synchronization may occur in heterogeneous phase distributions (e.g., Refs. [38–40]). Therefore, we will discuss a phase-synchronization index, which incorporates both the time dependance and the distribution of phases. In more detail, we will introduce a clustering method to detect quasistationary phase synchronization. As an extension of recent works [28,29], this method will allow for the segmentation of multivariate data by considering the spatio-temporal data structure comprising a cluster algorithm for phasic data

*Electronic address: hutt@wias-berlin.de
†Electronic address: marlow@fbw.vu.nl
‡Electronic address: u.steinmetz@mis.mpg.de

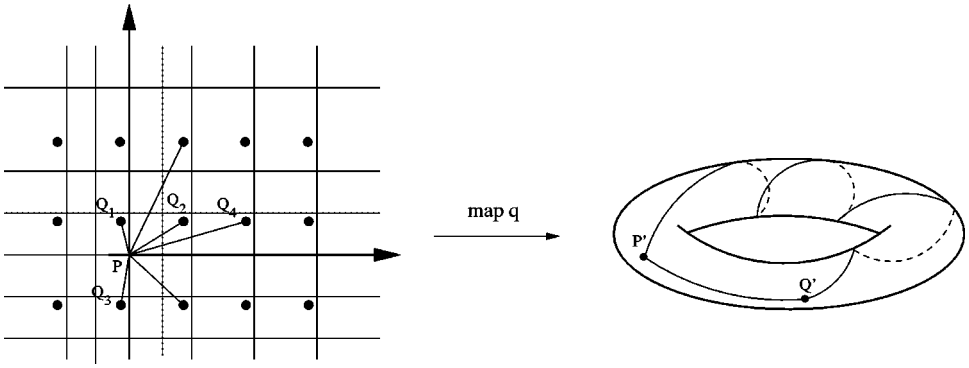

FIG. 1. Covering map q and nonuniqueness of geodesics. Points Q_i are mapped to a single point Q'. On the right-hand side, two geodesics are drawn, which correspond to two couples of points (P,Q_i). On the left-hand side, the dotted lattice represents the cuboid of mediatrices, which contains the point couple PQ_1 with the smallest distance on the torus.

as well as an average segmentation index for ensembles of time series. In particular, we will show in detail that the latter step reveals phase-synchronization properties of systems irrespective of specific realizations. Applications to nonstationary data obtained from both a stochastic model network and arrays of coupled Lorenz systems serve to illustrate our method.

The paper is structured as follows. In Sec. II, we discuss the topology of multivariate phasic data and derive major elements of a specific form of the *K*-means cluster algorithm as it will be used here. Applications to simulated data follow in Sec. III. Finally, we contrast our method to an existing bivariate synchronization index utilizing simulated data (Sec. III D).

II. METHODS

A. Clustering

To begin with, we recast multivariate signals as a temporal sequence of data points in high-dimensional data space, because in this picture quasistationary signals exhibit small variations in data space contrasting large changes during transient behavior. That is, small data variations result in high data point densities and, consequently, quasistationary signal states become visible as point clusters in data space [29]. In the context of time series of phases, quasistationary segments show bounded phase relations and, thus, follow from the definition of phase synchronization [41].

With this background, quasistationary multivariate signal states can be detected using conventional clustering algorithms. Without loss of generality, we utilize a *K*-means cluster algorithm and reformulate it in order to cope with cyclic data. Recall the explicit form of *K*-means clustering as described, e.g., in Ref. [42]: major algorithmic features are the computation of mean values and distances between data points. For nonperiodic data, variants of Euclidean distances, e.g., Mahalanobis or city-block distances [43], are commonly used for distance computation and mean values are determined by conventional averaging. These apparently simple computations can be used as long as the corresponding topological space is a plane and, accordingly, its metric is flat. In contrast, for cyclic data the topological space is a torus, whose *N*-dimensional geometrical realization is its embedding in $\mathcal{R}^{N+1}$, i.e., for $N=2$ the torus looks like the well-known doughnut. There, the shortest connection between two points is found on geodesics and distances have to be computed by solving the corresponding Euler-Lagrange equations. For curved metrics, however, solving the Euler-Lagrange equations becomes fairly difficult, in particular, for large N and/or for many point couples.

Again, irrespective of the explicit algorithm one uses to cluster the data one has to face the problem of computing distances between cyclic data. Fortunately, before utilizing rather costly solutions of Euler-Lagrange equations, some geometrical aspects readily help to find much simpler alternatives. Indeed, there exists a flat *N*-torus, whose geodesics are straight lines. Thus, with a covering map that reads

$$q:\mathcal{R}^N \rightarrow \mathcal{R}^N/\mathcal{Z}^N \sim \mathcal{T}^N$$

every geodesic in $\mathcal{R}^N$ projects to a geodesic on the *N*-torus $\mathcal{T}^N$ [44] as illustrated in Fig. 1. In consequence, distances on $\mathcal{T}^N$ can be computed as Euclidean distances in $\mathcal{R}^N$ at least when considering specific rules. Suppose we have arbitrary points denoted by $P,Q_i \in \mathcal{R}^N$ and their counterparts on the *N*-torus referred to as $P',Q' \in \mathcal{T}^N$. The map introduced above then reads $P'=q(P),Q'=q(Q_i)$ and, more specifically, we can determine the distance between P' and Q' as

$$d(P',Q') = \min_i [\overline{PQ_i}],$$

$\overline{\cdots}$ refers to Euclidean distances. In more physical terms, the correct Q_i is located in a cuboid of mediatrices around P (dotted line in Fig. 1) analogous to the calculation of Brillouin zones in solid state physics. Interestingly, the *N*-torus can be expressed as the (geometrical) product of *N* circles $\mathcal{S}^1$, i.e., $\mathcal{T}^N \sim \mathcal{S}^1 \times \cdots \times \mathcal{S}^1$ (N times). Consequently, the distance computation can be split into independent ones per component, each reflecting a circle. Distances, mean values, variances, etc., on a circle, however, are well documented so that, in sum, the distance between two data points P',Q' in a set of *N* dimensional phasic data obeys conventional rules of circular statistics—see, e.g., Ref. [45].

For our specific problem this geometrical aspect implies that for every given dataset $\{\boldsymbol{q}_i\}$ of *N* phase angles, each of which contains $i=1,\ldots,T$ data points (or time steps), i.e., $\boldsymbol{q}_i=(\phi_1^{(i)},\ldots,\phi_N^{(i)})^t$, distances between two arbitrary data points can be computed as follows:

$$d(\boldsymbol{q}_i,\boldsymbol{q}_j) = \sqrt{\sum_{k=1}^{N} d_k^2}, \tag{1a}$$

$$d_k = \pi - |\pi - |(\phi_k^{(i)} - \phi_k^{(j)}) \mathrm{mod} 2\pi||. \tag{1b}$$

As readily indicated, the means of periodic data can be computed for each phase angle independently by accounting for their circular properties [45]. Hence, we can finally calculate the mean value in terms of

$$\overline{\boldsymbol{q}} = \begin{pmatrix} \overline{\phi_1} \\ \vdots \\ \overline{\phi_N} \end{pmatrix}, \quad \tan\overline{\phi_k} = \frac{\sum_i \sin \phi_k^{(i)}}{\sum_i \cos \phi_k^{(i)}}. \tag{2}$$

Coming back to our main objective, that is, the *K*-means cluster algorithm, we are now in the position to determine cluster centers $\{\boldsymbol{C}_k\}$, $k=1,\ldots,K$. These centers refer to points in data space for which its mean distance to a (sub-)set of data points is minimal. Considering Eqs. (1) and (2), we modify the conventional *K*-means clustering so that it yields *K* cluster centers of phases. Here, it seems important to note that, in general, the proper number of clusters is unknown. In consequence, we define a quantity [27,28] that is motivated by the fact that the data in question represent time series and, thus, all the data are well ordered in time. Therefore, clusters can be considered as temporal segments as the *K*-means algorithm maps data points to their nearest cluster centers [29]. In the following, we associate a large and spatially well-separated data segment with a high cluster quality, whereas a small segment with overlapping clusters displays a low cluster quality. In more detail, for every number of clusters *K*, each data point *i* is associated with a cluster measure $A_K(i)$,

$$A_K(i) = \frac{1}{\mathcal{N}_K} \sum_{j \in \Omega_i} [d(\boldsymbol{C}_s, \boldsymbol{q}_j) - d(\boldsymbol{C}_n, \boldsymbol{q}_j)],$$

that is normalized by the factor $\mathcal{N}_K = \Sigma_{i=1}^{T} A_K(i)$. Here, $\boldsymbol{C}_n$ and $\boldsymbol{C}_s$ denote the nearest and the second-nearest cluster center of data point *i*, respectively. Ω_i represents a subset of members of the cluster to which data point *i* is associated. That is, the dataset is partitioned into distinct subsets Ω_i reflecting consecutive time segments each or, in turn, for every number of clusters *K* the subsets Ω_i represent consecutive time segments [28]. As mentioned before, the optimal number of clusters is unknown resulting in an uncertainty about a proper choice of *K*. To minimize this uncertainty we follow a statistical approach and average different cluster measures with increasing *K*. This procedure yields the so-called cluster quality measure

$$p(i) = \frac{\overline{A}(i)}{\mathcal{A}} \quad \text{with} \quad \overline{A}(i) = \frac{1}{R-1} \sum_{K=2}^{R} A_K(i)$$

with $\mathcal{A} = \Sigma_{i=1}^{T} \overline{A}(i)$ and value *R* reflecting the maximum number of clusters *R*. Indeed, an increasing number of clusters *K* yields an increasing number of subsets Ω_i and, subsequently, it diminishes the cluster measures $A_K(i)$. In other words, the quality measure $p(i)$ converges. Notice that, in general, an optimal value of the upper bound *R* depends on the real number of clusters in the data but *R* is usually in the range of tens.

In order to compare cluster qualities across different datasets, we further introduce a reference system by randomizing the examined dataset with respect to its temporal order and reapply the clustering algorithm. This procedure is similar to phase randomized surrogate data. Because the surrogates $p^{(s)}(i)$ do not contain any temporal structure they can be used to normalize the original values $p(i)$, see also Ref. [28] for more details. Thus, we define an effective clustering measure p_{eff} by means of

$$p_{\mathrm{eff}}(i) = \max\{0, p(i) - \max_j [p^{(s)}(j)]\}.$$

Anticipating the upcoming applications we realize that segment borders may show drastic increases and decreases of p_{eff} at their initial and final data points, respectively [27,28]. Hence, we finally extend the analysis by computing differences

$$\Delta p_{\mathrm{eff}}(i) = \max\{0, |p(i+1) - p(i)| - \max_j [|p^{(s)}(j+1) - p^{(s)}(j)|]\}$$

revealing significant peaks at segment borders.

B. Definition of phase

When studying time series, one typically includes some *a priori* knowledge or expectation about the underlying dynamical system. Investigating phase-synchronization effects, in particular, this *a priori* knowledge comes into play when defining the phase of interest (see, e.g., Ref. [41]). In many cases, however, such knowledge is simply not available so that general phase definitions have to be considered. Here, we apply the Hilbert transform with which the phase $\Phi(t)$ of a real signal $s(t)$ can be defined via its corresponding analytical signal $\tilde{s}(t)$, see, e.g., Ref. [46]:

$$\tilde{s}(t) = s(t) + iH(t), \tag{3a}$$

$$H(t) = \frac{1}{\pi} \mathrm{PV} \int_{-\infty}^{\infty} \frac{s(\tau)}{t-\tau} d\tau, \tag{3b}$$

$$\Phi(t) = \arctan\{H(t)/s(t)\}. \tag{3c}$$

The integral in Eq. (3b) refers to the Cauchy principal value. The Hilbert phase is widely used for studying phase synchronization in both simulated and experimental data [17,21–23,41,47], as it provides a phase measure that explicitly and instantaneously depends on time. Notice, however, that for physical interpretations this phase definition is only adequat for frequency band-limited data [48], i.e., limited variations of Poincaré return times. For instance, dynamics of chaotic systems exhibit a wide range of temporal scales. Hence, Hilbert phases of chaotic data are only valid for chaotic systems, whose parameters guarantee reduced variations of time scales.

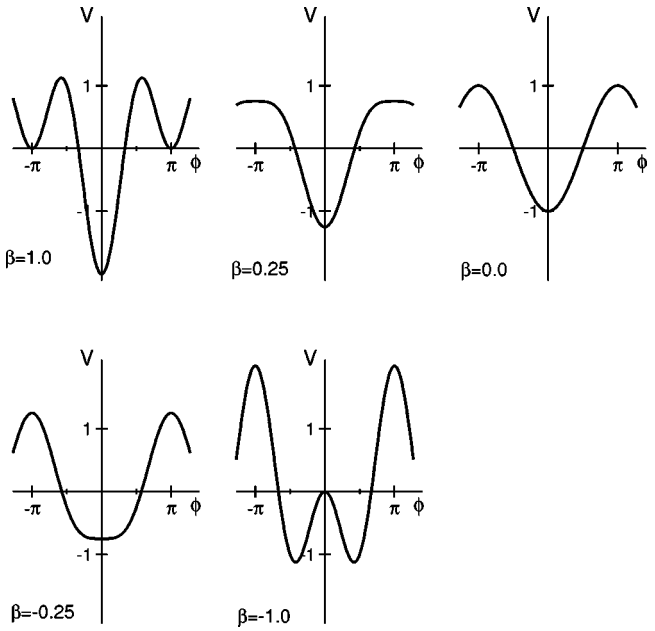

FIG. 2. Potential $V(\Phi)$ with $-\partial V/\partial\phi = -\sin\phi - \beta\sin 2\phi$ [cf. Eq. (4)] for different parameters β. States at $\phi = \pm\pi$ are unstable for $\beta < 0.25$, whereas $\phi = 0$ is unstable for $\beta < -0.25$

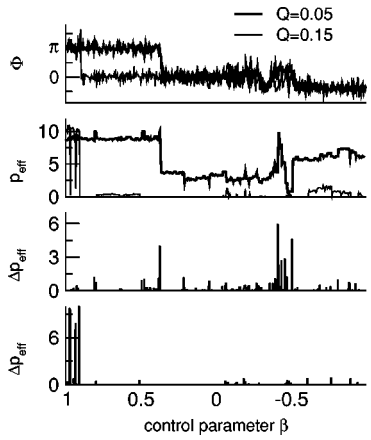

FIG. 3. Trials and clustering results for a single phase variable and two different noise levels Q. All the data are plotted with respect to the parameter β. The top panel presents the analyzed data and the middle panel displays the effective cluster quality measure. The two bottom panels contain the absolute value of the effective differential cluster quality measure. The unit of cluster quality measures is 1%.

III. APPLICATIONS

A. Simulated ensemble phase dynamics

First, we illustrate our method by use of the following stochastic dynamical system:

$$\frac{d\phi_k}{dt} = -\sin\phi_k - \beta\sin 2\phi_k + \sqrt{2Q}\Gamma_k, \tag{4}$$

where $k = 1, \ldots, N$. The values $\phi_k = \phi_k(t)$ represent phases that evolve along the gradient of a potential $V(\phi_k) = -\cos\phi_k - (\beta/2)\cos 2\phi_k$ (Fig. 2). Obviously, this potential prescribes a pitchfork bifurcation when changing the control parameter β. Additionally, the phases are individually subjected to additive Gaussian noise, for which we assume $\langle\Gamma_k(t)\rangle = 0$ and $\langle\Gamma_k(t)\Gamma_l(t')\rangle = 2\delta_{kl}\delta(t-t')$. For the sake of brevity, we abstain from a detailed discussion of this dynamics, but rather refer to the literature listed below. To motivate its use, however, note that this system is one of the minimal mathematical forms that allows for nontrivial scenarios of multivariate phase locking. As such, the potential terms on the right hand side are frequently used to model bistable phase dynamics as being found, for instance, in motor-behavior tasks [49]. That is, dependent on the relative values of the included parameters β and Q and dependent on its dimensionality N, this systems shows various forms of phase locking and/or bifurcation patterns.

To begin with, we discuss the univariate case by choosing $N = 1$. The dynamics reaches the vicinity of a certain potential minimum depending on the value of β. The width of the distribution around that minimum is given by the fluctuation strength Q. To change the location of the minimum, we subsequently vary the (control-)parameter β inducing a pitchfork bifurcation (cf. Fig. 2 and see, e.g., Refs. [49,50]). Note that in the following, we refer to a simulated solution of Eq. (4) as a trial being obtained by decreasing β from 1 to -1 in 500 equidistant steps. At each step the system relaxes for 1000 integrations and the final one is stored. Hence, the dataset contains only 500 points although the simulation comprises 500×1000 iterations. Put differently, we study the stochastic dynamics during a quasistatic variation of the control parameter β.

In Fig. 3, two simulated trials and the corresponding clustering results are shown for $Q = 0.05$ and $Q = 0.15$, respectively. In both cases, the initial phase angles were $\phi(0) = \pi$. The top panel displays the simulated data sets with phase switches at about $\beta = 0.35$ (thick line) and $\beta = 0.9$ (thin line) to a value around $\phi = 0$. The corresponding cluster quality measure (second row from top) exhibits rapid decreases at the corresponding values of β. Up to $\beta \approx -0.25$ the phases remain within the immediate vicinity of $\phi = 0$, which is followed by increasing fluctuations at both noise levels and subsequent steady states $\phi_0 \neq 0$ (cf. also Fig. 2). Especially for $Q = 0.05$, the latter change between $\beta = -0.25$ and $\beta = -0.55$ is reflected by rapid variations of the clustering measure $p_{\mathrm{eff}}(\beta)$. The final increase marks the border of the last data cluster [51] coinciding with the final phase variation. Although for $Q = 0.15$ significant jumps in $p_{\mathrm{eff}}(\beta)$ do not occur—here because of the large noise level—a short resting state is detected for the interval $\beta \in [-0.6; -0.95]$. In fact, a closer look at Fig. 2 helps to explain the fluctuations around $\phi = 0$ for $\beta \leqslant -0.25$: the potential minimum at $\phi = 0$ vanishes and turns into a (local) maximum. These qualitative changes can also be estimated by the clear peaks in the corresponding differential cluster quality measure Δp_{eff} that is displayed in the two bottom rows of Fig. 3.

Clustering results for multivariate data ($N = 50$) with $Q = 0.05$ are depicted in Fig. 4. Between $\beta = 1.0$ and $\beta = 0.77$, all the phase angles stay close to their initial values

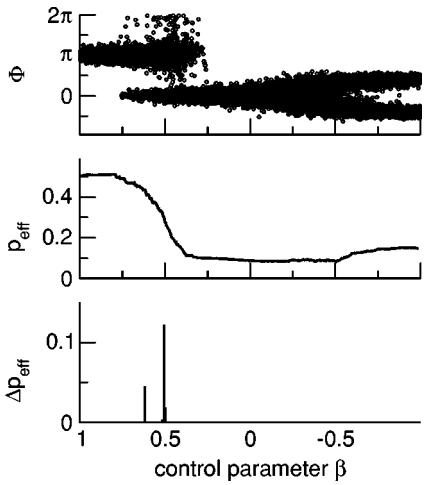

FIG. 4. Multidimensional data trial and clustering results for $N=50$ and noise level $Q=0.05$. All the data are plotted with respect to the parameter β. The top panel displays the data of N phase variables. The middle and bottom panels present the effective cluster quality measure and their corresponding differentials. The unit of cluster quality measures is 1%.

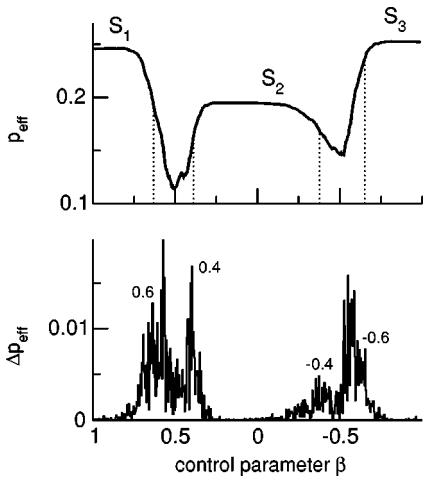

FIG. 5. Averaged clustering results for $N=50$, noise level $Q=0.05$ and 100 trials. The data are plotted with respect to the parameter β. The top panel displays the effective cluster quality measure and the bottom panel presents the corresponding differentials. The unit of cluster quality measures is 1%.

$\phi=\pi$ followed by $\pm\pi$ switches, i.e., $\phi=\pi\rightarrow\phi=0$ or $\phi=\pi\rightarrow\phi=2\pi$. Transitions occur around $\beta=0.5$, as can be determined via the cluster quality measure. p_{eff} is maximal in the interval $\beta\in[1.0;0.77]$ and decreases until β reaches 0.3 with a maximal slope at $\beta\approx0.5$. In line, the differential cluster quality measure $\Delta p_{\mathrm{eff}}(\beta)$ (Fig. 4, bottom row) has peaks in the transition regions. Actually, for $\beta<0.25$ only a subtle increase of p_{eff} can be observed near $\beta=-0.5$, which, however, does not show any nonvanishing differential cluster quality measure $\Delta p_{\mathrm{eff}}(\beta)$. Hence, we cannot distinguish this latter case from a random increase as might also be explained by the large noise strength, the small slope of the underlying potential, or the small distance between its minima. Notice that the figures of clustering results illustrate the spatiotemporal dynamics of data: quasistationary data with a large point density in data space reveal large values of p_{eff}, whereas transient and widely distributed data show low values. Only fast transitions between quasistationary data segments exhibit large peaks of Δp_{eff} implying that Δp_{eff} represents a transition likelihood to phase-synchronized states.

Underscoring its statistical relevance, we further examine an ensemble of 100 trials, each of which is computed with the aforementioned parameters. A subsequent application of the clustering method yields 100 time series of cluster quality measures and corresponding differentials, which will be averaged. Figure 5 displays plateaus of this mean cluster quality measure at segments S_1,S_2, and S_3 (top panel) and peaks of Δp_{eff} (bottom panel) reflect transition regions S_1-S_2 and S_2-S_3. We would like to point out that the nonvanishing peak widths reflect the duration of the transition regions and, at the same token, the uncertainty of segment borders. In more detail, we find $S_1=[1.0;0.6]$, $S_2=[0.4;-0.4]$, and $S_3=[-0.6;-1.0]$. The exact statistical assessment of our results, e.g., the estimation of peak variances, is beyond the scope of the present paper but will be addressed in future work.

This study shows mutual synchronization of uncoupled systems as being expected in the case of identical systems that have steady solutions. The result reveals the relation between the degree of synchronization (here in identical systems) and the stability properties of the participating subsystems: as soon as the transition rate within a system is high (e.g., close to instabilities) the (mutual) synchronization is low, whereas common steady states show high synchronization.

B. Weakly coupled Lorenz systems with external driving force

Evaluating our method with more irregular multivariate data, we continue with studying phase signals being obtained from chaotic data. Note that phase synchronization always occurs with respect to a phase reference. In general, however, multivariate signals do not serve as a unique reference and, therefore, we examine datasets including all couples of phase differences (this section) and phase differences of nearest neighbors (Sec. III C). The system in question is a ring of five diffusion-coupled Lorenz systems

$$\dot{x}_i=-10x_i+10y_i, \tag{5a}$$

$$\dot{y}_i=28x_i-y_i-x_iz_i+C(y_{i+1}+y_{i-1}-2y_i), \tag{5b}$$

$$\dot{z}_i=x_iy_i-\tfrac{8}{3}z_i+F(t), \quad i=1,\ldots,5, \tag{5c}$$

driven by an external force $F(t)=10\sin(8.3t)$. This system yields the so-called imperfect phase synchronization for vanishing coupling [13], i.e., the phase of every single attractor drifts in short segments by multiples of 2π relative to the external force $F(t)$. This drifting is caused by the broad range of intrinsic scales of the Lorenz system.

We realized numerical solutions of Eq. (5) by applying an Euler-forward algorithm with step size 0.01, where uniformly distributed initial values $(x_i(0),y_i(0),z_i(0))=(8.4$

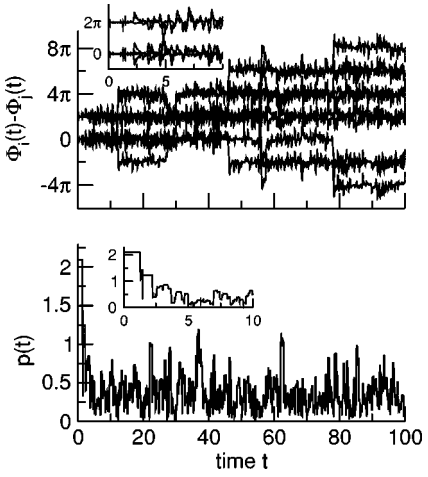

FIG. 6. Time series of phase differences and obtained cluster quality measure for uncoupled Lorenz systems driven by an external force. Insets zoom into smaller time windows to enlarge details. The unit of cluster quality measures is 1%.

$+\Gamma_x, 8.4+\Gamma_y, 40+\Gamma_z)$ with $\Gamma_{x,y,z} \in [-0.5;0.5]$ guaranteed a stable integration of $T=15\,000$ time steps.

Figure 6, top panel, displays time series of ten Hilbert phase pairs $\Delta\Phi_{ij}=\Phi_i-\Phi_j$ of amplitudes $\{y_i\}$ in the case of vanishing coupling ($C=0$) showing the aforementioned characteristic phase slips. Since the individual phases drift at random points in time, no mutual phase synchronization is present. This is reflected by the absence of any prominent structure of the corresponding cluster quality measure (Fig. 6, bottom panel). Because of similar initial values, the five Lorenz systems synchronize briefly at the beginning of the simulation, after which the cluster quality measure drops rapidly (cf. inset of Fig. 6, bottom panel). To examine the influence of coupling strength C, we further computed averages of 15 trials (Fig. 7) for various values of C. By increasing the coupling strength, phase synchronization increases and spreads in time. Hence, increased coupling stabilizes the phase relation of attractors, at least for a finite time, and the averaged differential cluster quality measures (Fig. 7, right hand side) show sharp peaks and gaps.

Indeed, more detailed investigations of single trials show that phase drifts relative to the external stimulus appear to remain present for $C\neq 0$. That is, within a finite time window, phases of the attractors still appear to *climb a staircase of phases mutually* by multiples of 2π. However, they align only for a certain time, after which this mutual phase synchronization disappears.

C. Strongly coupled Lorenz systems with strong external noise

As already mentioned in the preceding section, we further examine phase differences to the nearest neighbors—now, we consider the case of a chaotic system defined as a ring of eight diffusion-coupled Lorenz systems, that is, for $i=1,\ldots,8$ we have

$$\dot{x}_i = -10x_i + 10y_i + \Gamma_x, \tag{6a}$$

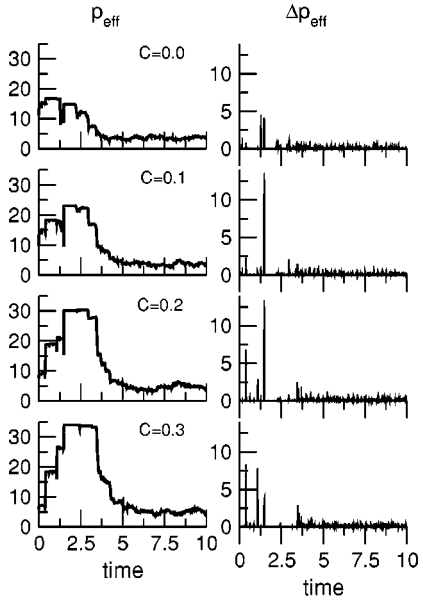

FIG. 7. Results for different coupling strengths C in coupled Lorenz systems driven by external force. The left column contains cluster quality measures averaged over 15 trials and the right side shows their corresponding differentials. The unit of cluster quality measures is 1%.

$$\dot{y}_i = 28x_i - y_i - x_i z_i + 3.0\cdot(y_{i+1}+y_{i-1}-2y_i) + \Gamma_y, \tag{6b}$$

$$\dot{z}_i = x_i y_i - \tfrac{8}{3} z_i + \Gamma_z, \tag{6c}$$

with strong external noise $\Gamma_{x,y,z} \in [-4.0;4.0]$ subject to a uniform distribution. Initial conditions and integration procedure are identical to the previous study. Recall that we examine phase differences to the nearest neighbors, which yields an eight-dimensional time series of phases.

Concentrating on phases from the amplitudes $\{y_i\}$, Fig. 8 shows three single time series of phase differences $\Delta\Phi_{ij}$. In trials 2 and 3, we find early transitions to fairly stationary phase relations, contrasting trial 20, which exhibits several switches of multiples of 2π. This differential behavior is caused by both different initial conditions and external noise. The corresponding cluster quality measures for all trials confirm these findings by transients and plateaus in the according time segments. We point out that the low values of p_{eff} indicate either large intersecting clusters or clusters of only few aggregated data, both reflecting weak phase synchronization. In order to decide whether there is coincidental phase synchronization in trials, we computed an average cluster quality measure over 20 trials (Fig. 8, bottom panel) that exhibits several peaks and troughs. For instance, both from $t=80$ to $t=90$ and for $t>90$, the plateaus indicate coincidental mutual phase synchronization across trials.

Next, we examined the phase-synchronized state in more detail. Figure 9 shows signal amplitudes of all trials from Fig. 8 as space-time plots, which reveal alternations between phase synchronization and desynchronization. For instance, in trial 2, one can find final steady-state oscillations with vanishing phase lags between couples 1-8, 2-7, 3-6, and 4-5

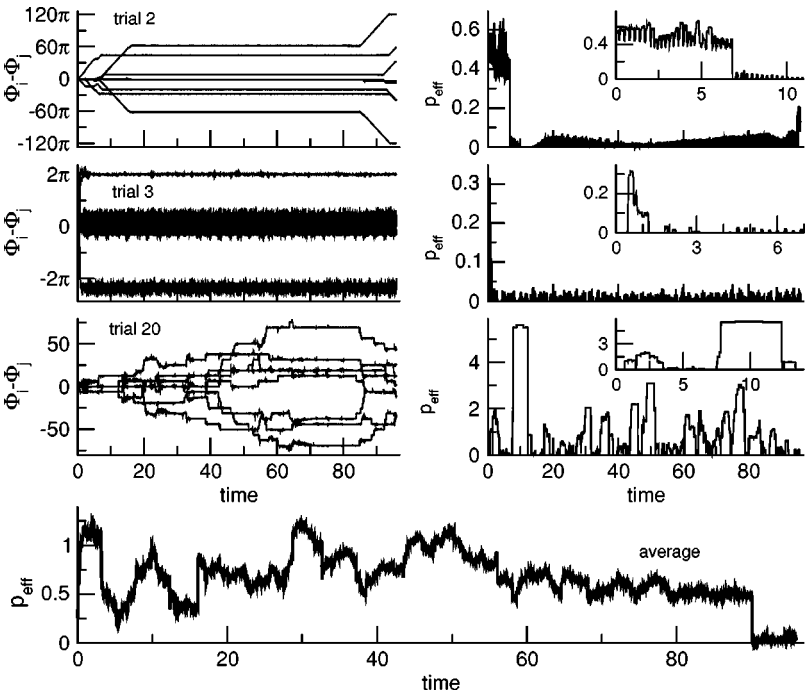

FIG. 8. Time series of phase differences obtained from amplitudes $\{y_i\}$ and corresponding cluster quality measures in the case of strongly coupled Lorenz systems. Plot insets in the right column focus upon time windows from Fig. 9 to reveal more details. The bottom panel shows averaged cluster quality measures obtained from further 20 trials. The unit of cluster quality measures is 1%.

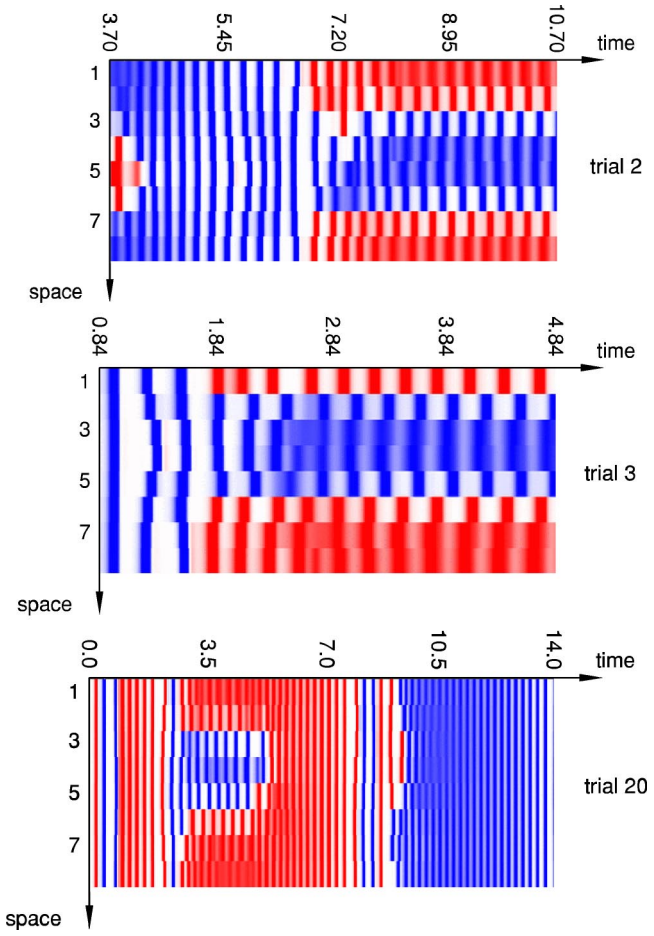

FIG. 9. Space-time plots of amplitudes $\{y_i\}$ of trials in Fig. 8.

symmetric to points between 4,5 and 1,8. The noise-free variant of system (6) possesses an invariant linear manifold $\{x_{5+i}=x_{4-i}, y_{5+i}=y_{4-i}, z_{5+i}=z_{4-i}, i=1,\ldots,4\}$, and three rotated copies thereof corresponding to the successive pairs of nodes (cf. [39]) and containing locally asymptotic stable limit cycles. A similar spatiotemporal symmetry occurs in trial 3, however, shifted by one element. In trial 20, quasistationary phases constant in space alternate with stripe patterns, whereas no symmetric pattern is present similar to the ones in trials 2 and 3. In all the trials, plateaus of p_{eff} show good accordance in time to segments of quasistationary

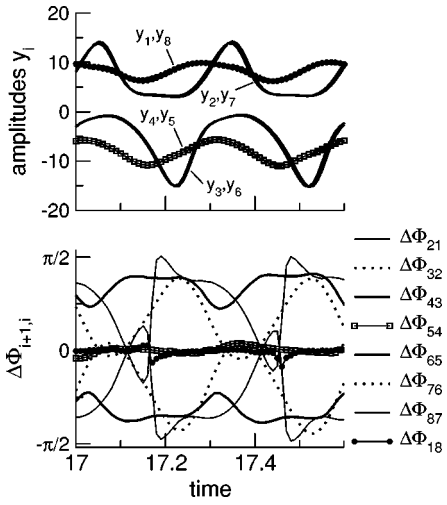

FIG. 10. Single amplitudes $\{y_i\}$ and corresponding phases of trial 2 in Fig. 8. For instance, plots of amplitudes marked by dots and squares in the top panel correspond to curves with approximately zero phase lag shown in the bottom panel.

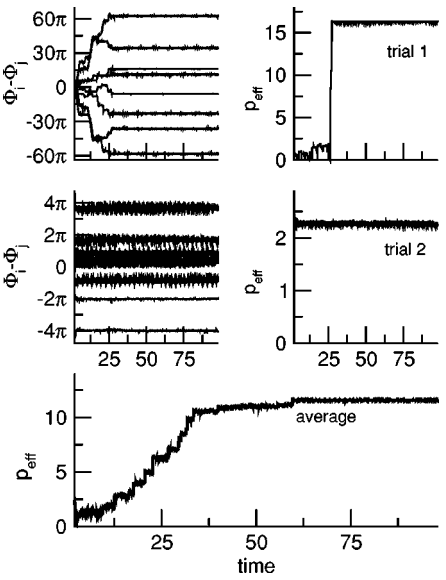

FIG. 11. Time series of phase differences obtained from amplitudes $\{z_i\}$ and corresponding cluster quality measure in case of strongly coupled Lorenz systems. The bottom panel shows averaged cluster quality measures obtained from further 20 trials.

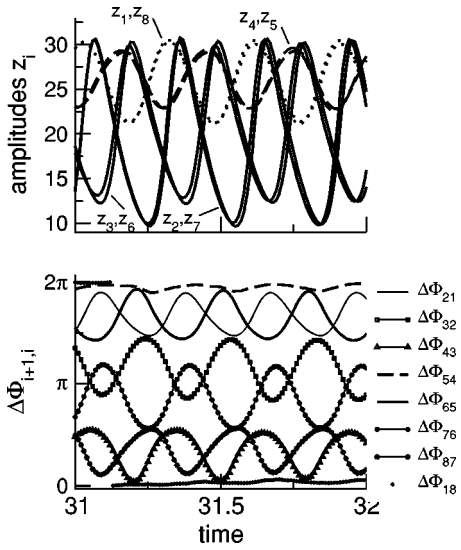

FIG. 12. Single amplitudes $\{z_i\}$ and corresponding phases of trial 1 in Fig. 11. For instance, plots of amplitudes marked by dots and dashes in the left panel correspond to curves with phase lag 0 and 2π shown in the right panel.

phase synchronization (cf. insets in Fig. 8). Figure 10 depicts amplitudes and their corresponding phase differences $\Delta\Phi_{(i+1)i}$ of the phase-synchronized state and illustrates the observed mirror symmetry. Here, the plots indicate the well-known nonsinusoidal behavior in amplitudes $\{y_i\}$ yielding large fluctuations of the corresponding phases and, subsequently, weak phase synchronization.

Different results can be obtained when considering amplitudes $\{z_i\}$ in Eq. (6). Figure 11 shows time series of corresponding phases in two trials (left panels) that reveal transients on different time scales and final stationary phase differences. Apparently, these differences in time scales result from different initial conditions and the applied external noise.

Finally, we computed the cluster quality measures for both trials (right panels) and the average over 20 further trials (bottom panels). For the single trials, the cluster quality measures reveal transients and plateaus in accordance with the time series of phase differences. The average cluster quality measure increases from low values of p_{eff} and saturates at about $t=30$ (bottom panel, left hand side). Interestingly, these clear structures contrast with the alternating ones from the amplitudes $\{y_i\}$. In Fig. 12 we show the amplitudes and the corresponding phase pairs of the phase-synchronized state. The phase relations change periodically within a narrow phase band implying that the data cover a bounded region in data space and, hence, represent (by definition) a phase-synchronized state [41].

D. Comparison to bivariate synchronization index

At last, we compare our method with a synchronization index being discussed by Rosenblum *et al.* [36]. In case of 1:1 phase locking, Rosenblum and co-workers proposed an index that represents the circular standard deviation of phase differences $\{\Delta\Phi_{ij}(t)\}$ and that reads

$$\gamma_{ij}(t)=\sqrt{\langle\cos\Delta\Phi_{ij}(t)\rangle^2+\langle\sin\Delta\Phi_{ij}(t)\rangle^2} \tag{7}$$

with $i,j=1,\ldots,N$. $\langle\cdots\rangle$ denotes an average over a time window $[t-\Delta T/2;t+\Delta T/2]$. Due to definition (7), large values of $\gamma_{ij}(t)$ indicate a narrow-peaked unimodal distribution of phase differences, whereas $\gamma_{ij}(t)\to 0$ reflects a uniform distribution. Notice that, since this synchronization index only applies to bivariate data, that is, to single phase differences, we extend it by computing the simple mean synchronization index over all the phase differences of nearest neighbors

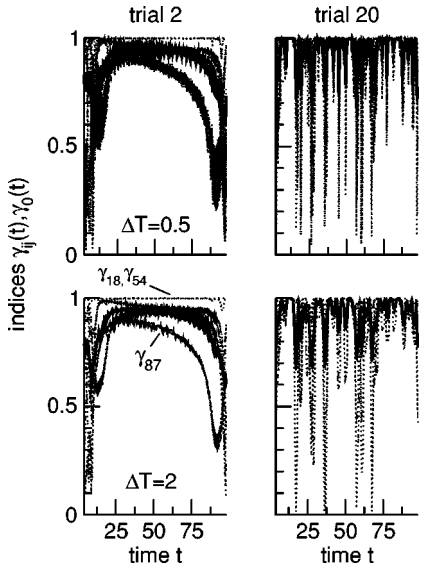

FIG. 13. Bivariate phase-synchronization indices of amplitudes $\{y_i\}$ in Fig. 8 for different trials and values of ΔT. Dotted lines, eight indices $\gamma_{(i+1)i}(t)$; bold solid lines, index $\gamma_0(t)$.

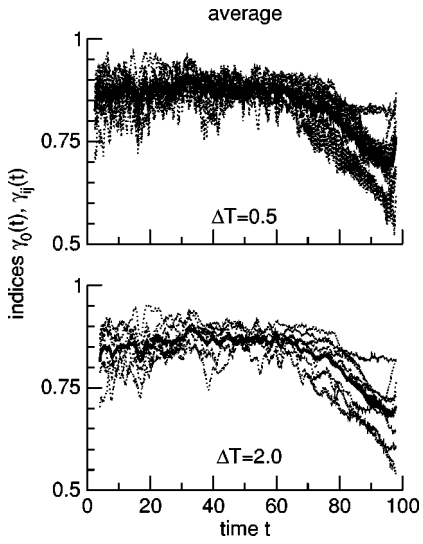

FIG. 14. Averaged bivariate phase-synchronization indices of amplitudes $\{y_i\}$ in Fig. 8 for different values of ΔT. Dotted lines, eight averaged indices $\gamma_{(i+1)i}(t)$; bold solid lines, averaged index $\gamma_0(t)$.

$$\gamma_0(t)=\frac{1}{N}\sum_{i=1}^{N}\gamma_{(i+1)i}(t), \quad \gamma_{(N+1)N}=\gamma_{1N}.$$

Applying this form to phases of the amplitudes $\{y_i\}$ from the previous study yields eight time series of synchronization indices shown in Fig. 13 for two different trials and two different time spans ΔT, respectively. We find large values and troughs of $\gamma_0(t)$ in time segments similar to our results, while single indices $\gamma_{ij}(t)$ diverge from each other. For instance, in trial 2 we observe $\gamma_{54},\gamma_{18}\approx 1$ (Fig. 13, left panels), whereas values of γ_{87} reach a minimum of 0.6 at about $t=13$. In contrast, our method (Fig. 9) reveals mutual phase synchronization beyond $t>7.3$.

Since the bivariate synchronization index does account for mutual increases and decreases of the single circular standard deviations which also represents phase-locked behavior, it entirely neglects the spatiotemporal structure of the data and, thus, fails in detecting mutual phase synchronization. Allowing for a direct comparison with our studies, we finally computed synchronization indices averaged over trials. Figure 14 shows results for two values of ΔT indicating strong synchronization at all times. These findings contrast our aforementioned results, which show peaks and distinct borders of phase-synchronized segments.

IV. DISCUSSION AND CONCLUSION

We examined the structure of phasic data in high-dimensional spaces. In general, data clusters represent phase-synchronized states so that members of clusters build time segments of phase-synchronized states. Our method accounts for the spatio-temporal structure of data and is invariant towards constant offsets so that it seems reasonable to average clustering results over trials. In the case of small trial numbers, the average cluster quality measure reflects coinciding phase synchronization across the trial ensemble and, therefore, it allows for qualitative investigations of sets of chaotic systems. For large numbers of realizations, the differential cluster quality measure can be used to determine the distribution of transients between phase-synchronized segments.

Classically, bivariate synchronization indices facilitate the detection of phase synchronization between single phase couples and help to estimate properties of their statistical distribution in time. The corresponding time series of indices reveal smooth transients subject to the applied time window. With these indices one extracts temporal segments of quasistationary phase synchronization solely based on individual phase differences. In contrast, our method does not resolve phase synchronization in single phase couples, but rather detects mutual phase synchronization across all phases. This aspect is particularly important in spatially extended systems, which exhibit strong correlation in space, i.e., with huge sets of recorded time series. In addition, our method yields sharp borders of segments, and, hence, it allows for extracting initial and final time points of mutual phase synchronization.

In summary, the present work describes a segmentation index for mutual phase synchronization in multivariate nonstationary signals. With this segmentation index we are able to detect both the time segments and the duration of transients irrespective of the specific type of spatial synchronization patterns. Applications to stochastic phasic data and time series from coupled chaotic systems reveal the proposed index being able to capture the spatiotemporal structure of data.

ACKNOWLEDGMENTS

A.H. would like to thank P.J. Beek and the Faculty of Human Movement Sciences, Vrije Universiteit, Amsterdam, for their kind hospitality and their financial support. A.H. was also supported by the DFG Research Center ''Mathematics for key technologies'' in Berlin, Germany.

[1] *Analysis of Neurophysiological Brain Functioning*, edited by C. Uhl (Springer, Berlin, 2001).
[2] M. Rugg and M. Coles, *Electrophysiology of Mind* (Oxford University Press, Oxford, 1996).
[3] E. Bazar, *Brain Function and Oscillations* (Springer, Berlin, 1998).
[4] Y. Kuramoto, *Chemical Oscillations, Waves, and Turbulence* (Springer, Berlin, 1984).
[5] *An Introduction to Dynamic Meteorology*, edited by J. Holton, (Academic Press, New York, 1992).
[6] *Elastic Waves in Random Media*, edited by S. Shapiro and P. Hubral (Springer, Berlin, 1999).
[7] *Principles of Optics*, edited by M. Born and E. Wolf (Cambridge University Press, New York, 1999).
[8] D. Brandeis, D. Lehmann, C. Michel, and W. Mingrone, Brain Topogr **8**, 145 (1995).

[9] F. Busse and K. Heikes, Science **208**, 173 (1980).
[10] J. Rodriguez, C. Perez-Garcia, M. Bestehorn, M. Frantz, and R. Friedrich, Phys. Rev. A **46**, 4729 (1992).
[11] C. Kim, K. Lee, J. Kim, S. Kwon, C. Kim, and J. Lee, J. Opt. Soc. Am. B **10**, 1651 (1993).
[12] T. Heil, I. Fischer, W. Elsaesser, J. Mulet, and C. Murasso, Phys. Rev. Lett. **86**, 795 (2001).
[13] M. Zaks, E. Park, M. Rosenblum, and J. Kurths, Phys. Rev. Lett. **82**, 4228 (1999).
[14] Z. Liu, S. Chen, and B. Hu, Phys. Rev. E **59**, 2817 (1999).
[15] W. Singer and C. Gray, Annu. Rev. Neurosci. **18**, 555 (1995).
[16] K. Lee, L. Williams, M. Breakspear, and E. Gordon, Brain Res. Rev. **41**, 57 (2003).
[17] P. Tass, *Phase Resetting in Medicine and Biology: Stochastic Modelling and Data Analysis* (Springer, Berlin, 1999).
[18] H. Haken, *Brain Dynamics* (Springer, Berlin, 2002).
[19] M. Zhang, G. Wei, and C.-H. Wei, Phys. Rev. E **65**, 036202 (2002).
[20] L. Pecora and T. Carroll, Phys. Rev. Lett. **80**, 2109 (1998).
[21] M.G. Rosenblum, A.S. Pikovsky, and J. Kurths, Phys. Rev. Lett. **76**, 1804 (1996).
[22] A. Pikovsky, M. Rosenblum, and J. Kurths, *Synchronization: A Universal Concept in Nonlinear Sciences* (Cambridge University Press, Cambridge, England, 2001).
[23] S. Boccaletti, J.K.G. Osipov, D. Valladares, and C. Zhou, Phys. Rep. **366**, 1 (2002).
[24] J. Wackermann, Int. J. Psychophysiol. **34**, 65 (1999).
[25] R. Pascual-Marqui, C. Michel, and D. Lehmann, IEEE Trans. Biomed. Eng. **42**, 658 (1995).
[26] R. Ihl and J. Brinkmeyer, Dement Geriatr. Cogn Disord. **10**, 64 (1999).
[27] A. Hutt and F. Kruggel, in *Space-Time Chaos: Characterization, Control and Synchronization*, edited by S. Boccaletti, H. Mancini, W. Gonzales-Vias, J. Burguete, and D. Valladares (World Scientific, Singapore, 2001), pp. 29–44.
[28] A. Hutt and H. Riedel, Physica D **177**, 203 (2003).
[29] A. Hutt, M. Svensen, F. Kruggel, and R. Friedrich, Phys. Rev. E **61**, R4691 (2000).
[30] H. Haken, *Advanced Synergetics* (Springer, Berlin, 1983).
[31] P. Tass, M. Rosenblum, J. Weule, J. Kurths, A. Pikovsky, J. Volkmann, A. Schnitzler, and H.-J. Freund, Phys. Rev. Lett. **81**, 3291 (1998).
[32] A. Daffertshofer, C.E. Peper, and P.J. Beek, Phys. Lett. A **266**, 290 (2000).
[33] A. Fuchs, J. Mayville, D. Cheyne, H. Einberg, L. Deeke, and J. Kelso, Neuroimage **12**, 71 (2000).
[34] A. Haig, E. Gordon, J. Wright, R. Meares, and H. Bahramali, NeuroReport **11**, 669 (2000).
[35] S. Slewa-Younan, A. Green, I. Baguley, K.L. Felmingham, A. Haig, and E. Gordon, J. Clin. Neurophysiol. **113**, 1640 (2002).
[36] M. Rosenblum, A. Pikovsky, C. Schafer, P. Tass, and J. Kurths, in *Handbook of Biological Physics, Neuroinformatics*, Vol. 4, edited by F. Moss and S. Gielen (Elsevier, New York, 2000), pp. 279–321.
[37] D. DeShazer, R. Breban, E. Ott, and R. Roy, Phys. Rev. Lett. **87**, 044101 (2001).
[38] S. Yanchuk, Y. Maistrenko, and E. Mosekilde, Math. Comput. Simul. **54**, 491 (2001).
[39] V. Belykh, I. Belykh, and M. Hasler, Phys. Rev. E **62**, 6332 (2000).
[40] V. Belykh, I. Belykh, and E. Moskilde, Phys. Rev. E **63**, 036216 (2001).
[41] A. Pikovsky, M. Rosenblum, and J. Kurths, Int. J. Bifurcation Chaos Appl. Sci. Eng. **10**, 2219 (2000).
[42] J. Moody and C.J. Darken, Neural Comput. **1**, 281 (1989).
[43] K. V. Mardia, J. T. Kent, and J. M. Bibby, *Multivariate Analysis* (Academic Press, London, 1979).
[44] S. Gallot, D. Hulin, and J. Lafontaine, *Riemannian Geometry* (Springer, Berlin, 1987).
[45] K. Mardia, *Statistics of Directional Data* (Academic Press, London, 1972).
[46] D. Gabor, J. IEE (London) **93**, 429 (1946).
[47] A. Pikovsky, M. Rosenblum, G. Osipov, and J. Kurths, Physica D **104**, 219 (1997).
[48] N. Huang, Z. Shen, S. Long, M. Wu, H. Shih, Q. Zheng, N. Yen, C. Tung, and H. Liu, Proc. R. Soc. London, Ser. A **454**, 903 (1998).
[49] G. Schner, H. Haken, and J. Kelso, Biol. Cybern. **53**, 247 (1986).
[50] H. Haken, J.A.S. Kelso, and H. Bunz, Biol. Cybern. **51**, 347 (1985).
[51] With respect to the forthcoming discussion about multivariate signals, we here maintain the notation for data ''clusters'' although for univariate data the phrase ''segment'' seems more appropriate.